Proceedings World Geothermal Congress 2023
Beijing, China, April 17 – 21, 2023

Connecting high- and low-pressure geothermal wells using an ejector: Analysis of first field tests at the Theistareykir Geothermal Power Plant

Ximena Guardia Muguruza[1], Jeffrey Macatangay Andal[1,3], Ragnar Lárusson[1], Guðrún Sævarsdóttir[1], Yonatan Afework Tesfahunegn[1], Egill Júlíusson[1], Vijay Chauhan[1,3], Karl E. Sveinsson[2], María Sigríður Guðjónsdóttir[1,3]

[1] Department of Engineering, Reykjavik University, Menntavegur 1, 102 Reykjavik, Iceland.

[2] Landsvirkjun, Háaleitisbraut 68, 103 Reykjavík, Iceland.

[3] GRO-GTP, Urdarhvarf 8, 203 Kópavogur, Iceland.

ximena21@ru.is

Keywords: Ejector, geothermal energy, thermodynamics

ABSTRACT

An ejector is a piece of equipment that uses high-pressure fluid to induce fluid flow from a low-pressure source, resulting in an intermediate common outlet pressure or back pressure. Ejectors are used extensively in the oil and gas, chemical, nuclear, aeronautics, fuel cells, desalinisation, and refrigeration industries. In the geothermal sector, ejectors are used mainly to extract non-condensable gases from power plant condensers. However, no successful use of ejectors to induce geothermal fluid from low-pressure wells has been reported in the literature.

An ejector was placed at the Theistareykir Geothermal Power Plant in 2021 to test if the high-pressure fluid from well ThG-11 could induce flow from the low-pressure well ThG-15. Pressure and temperature gauges, vortex meters, and orifice plates were used to measure pressure, temperature, enthalpy, and mass flow in different parts of the set-up. In this study, the measured data were analysed to determine under what flow conditions the ejector induced fluid from well ThG-15. An analytical model of the tested ejector was developed to explain how the system operates and to predict the ejector's flow properties, such as enthalpy, pressure, entropy, and velocity for all the data sets. Finally, the results of the analytical model were compared to the test data.

1. INTRODUCTION

Geothermal production wells are susceptible to pressure decline over time, which could make them unusable for power generation when their pressure drops below the operating conditions of the steam gathering system for the power plant. This situation could decrease the plant's power output, generating the need for drilling make-up wells with considerable capital cost.

In 2021, Landsvirkjun tested an ejector at its Theistareykir Geothermal Power Plant in Northeast Iceland to see if the high-pressure fluid from well ThG-11 could induce flow from the low-pressure well ThG-15. Well ThG-11 is a directional well of 2224 m depth located on well pad B and is currently producing 14.4 MWe on average, whereas well ThG-15 is also a directional well of 2260 m depth situated on the same well pad but is currently not in production (Hardarson et al., 2021), (Mkangala, 2021).

Well ThG-11 delivers superheated steam with an estimated enthalpy at or above 2800 kJ/kg and a wellhead pressure (WHP) ranging from 33 to 41 bar-g. Well ThG-15 delivers low-pressure fluid with an estimated enthalpy of 950 kJ/kg, a maximum wellhead pressure of 10 bar-g and a steam quality of 8,4%[1]; however, the well does not deliver much at this WHP and is susceptible to choking as a result of occasional pressure pulses that may run along the main steam pipeline. During the tests executed in 2021, both wells were connected through an ejector. In this study, we analyse the data gathered during the ejector's tests and compare it to results from an analytical model.

2. EJECTOR TESTS AT THE THEISTAREYKIR GEOTHERMAL POWER PLANT

Figure 1 shows the schematic locations of wells, ejector, pressure gauges, vortex meters, and orifice plates of the test conducted in 2021. In the current analysis, pressure measurements at the ejector's primary inlet (flow from ThG-11), secondary inlet (from ThG-15), and outlet are taken from gauges EJEC_HP, EJEC_LP, and ORF1-P1, respectively.

[1] Data provided by Landsvirkjun, 2022.

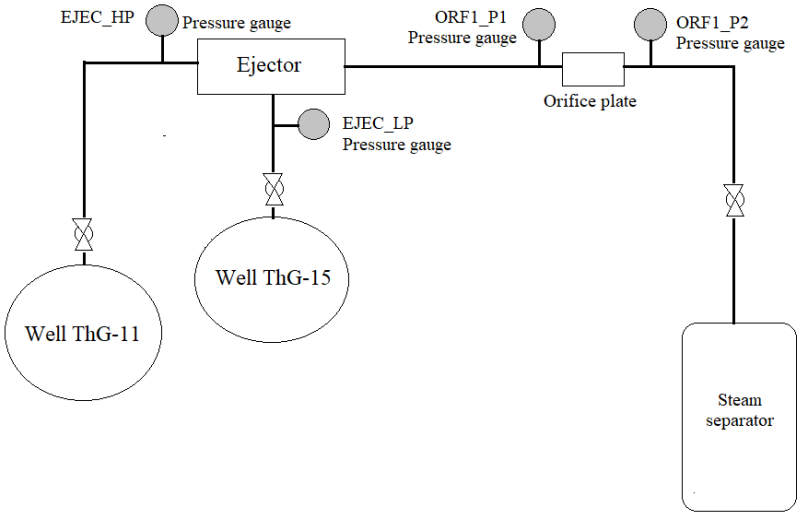

Figure 1. Set-up schematic of the test executed at the Theistareykir Geothermal Power Plant.

Test runs started by setting the desired mass flow rate from well ThG-11 with the pipeline fully open to the separator, and when the desired mass flow rate was reached, the wellhead valve of well ThG-15 was fully opened. Once stable conditions were achieved, the back pressure was adjusted manually using a valve located just upstream of the steam separator.

2.1 Design of the ejector tested at the Theistareykir Geothermal Power Plant

The ejector tested at the Theistareykir Geothermal Power Plant was composed of a suction chamber with a converging nozzle inside, a mixing chamber, and a diffuser, as shown in Figure 2. In contrast to most ejector designs, it did not have a constant area mixing section as part of the mixing chamber.

Reference points for each principal component of the ejector are described as follows:

1. Entrance of primary flow into the nozzle.
2. Converging nozzle's outlet.
3. Primary flow at the mixing chamber.
4. Entrance of secondary flow.
5. Secondary flow at the mixing chamber.
6. Mixed flow in the mixing chamber.
7. Mixed flow in the throat of the mixing chamber.
8. Mixed flow at the outlet of the ejector.

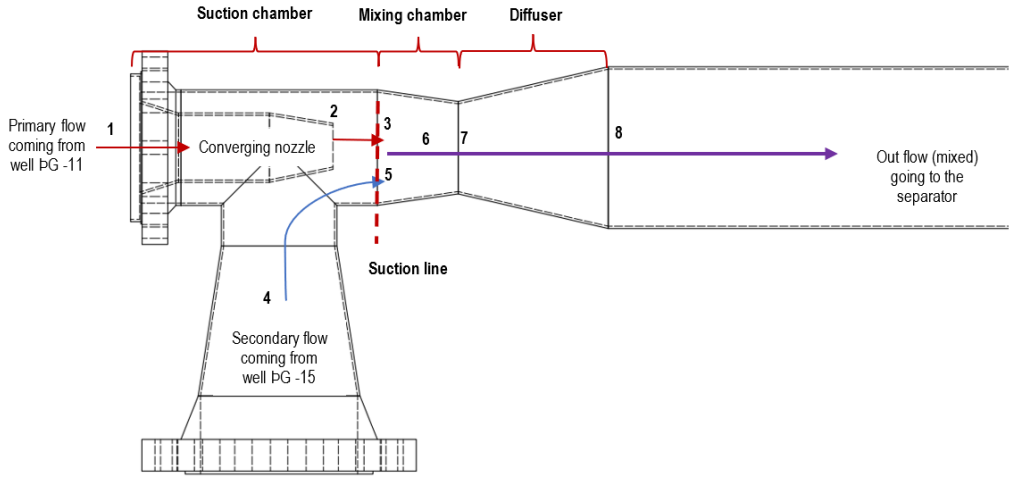

Figure 2. The ejector tested at the Theistareykir Geothermal Power Plant and reference points for the analytical model

3. ANALYTICAL MODEL OF THE EJECTOR TESTED AT THE THEISTAREYKIR GEOTHERMAL POWER PLANT

To develop an analytical model of the tested ejector, some assumptions were made based on the literature available for ejectors used in various industries. The motivation for developing this model is to understand the processes inside the ejector and assess its ability to predict its outlet enthalpy and pressure for given primary and secondary inlet conditions.

The following modelling assumptions were made:

- Even though the fluid is not an ideal gas, the model is based on available analytic equations for ideal gas to maintain the momentum balance, using a constant specific heat ratio $k = 1.33$. It is essential to mention that k could have a moderate change for significant temperature variations; however, the value used fits well for a temperature range between 250 and 1000 K. Therefore, constant specific heat is assumed for the analysis (White, 2011).
- The primary flow is saturated steam with high steam quality; consequently, the model uses density, enthalpy, pressure, and temperature values for this condition.
- The secondary flow is a mixture of liquid water and steam. However, the model treats it as a homogenous mixture (i.e., it uses weighted density and enthalpy, and a common pressure and temperature for the phases).
- Isentropic relations are used to simplify the analytical model derivation. However, to account for non-ideal processes, a loss coefficient is used. The coefficient for mixing and friction loss $c_{l,}$ is taken from (Huang, Chang, Wang, & Petrenko, 1999), with $c_l = 0.84$ for an area ratio[2] less than 6.9. The isentropic efficiency of the nozzle is $\eta_n = 0.9$.
- The primary and the secondary flow mix in the mixing chamber before reaching the mixing chamber's throat (7). The mixing is assumed to occur at a uniform pressure equal to the pressure of the secondary flow (5).
- The kinetic energy at the secondary flow entrance (4), primary nozzle entrance (1), and diffuser outlet (8) is negligible.
- There is no heat loss through the ejector walls.
- Effects of the liquid-vapour phase change (i.e., condensation and boiling) are not accounted for in the model.

Where the ideal gas assumption is not necessary for the model, CoolProp (Bell, Wronski, Quoilin, & Lemort, 2014) was used in the current study to obtain steam/water thermodynamic properties according to the IAPWS-95 formulation (IAPWS).

3.1 Equations for the different sections of the ejector

Converging nozzle (2)

Velocity is disregarded at the primary nozzle inlet (1). The Mach number at the nozzle exit (2) is obtained with the area Mach number relation (Anderson, 2021):

$$\frac{A_2}{A_2^*} = \frac{1}{M_2}\left[\frac{1+\frac{1}{2}(k-1){M_2}^2}{\frac{1}{2}(k+1)}\right]^{\frac{k+1}{2(k-1)}} \tag{1}$$

The pressure at the nozzle exit (p_2) can be calculated using isentropic relation:

$$\frac{p_{2-0}}{p_2} = \left[1+\frac{1}{2}(k-1){M_2}^2\right]^{\frac{k}{k-1}} \tag{2}$$

Where p_{2-0} is the stagnation pressure.

Given the isentropic efficiency η_n of the compressible flow in the nozzle and the isentropic enthalpy h_2^* obtained from the calculated pressure and entropy, h_2 can be calculated as follows:

$$h_2 = h_1 - \eta_n(h_1 - h_2^*) \tag{3}$$

Suction line (3 and 5)

It is assumed that the properties of the secondary flow are constant from the inlet up to the suction line:

$$p_5 = p_4\ ,\ h_5 = h_4\ ;\ T_5 = T_4\ ,\ s_5 = s_4\ ,\ \rho_5 = \rho_4\ ,\ v_5 = v_4 \tag{4}$$

It is further assumed that the entropy of the primary flow remains constant from the outlet of the nozzle (2) to the suction line (3) and that the two streams start to mix with uniform pressure, equal to the pressure of the secondary fluid at the suction line (5):

$$s_2 = s_3 \quad p_5 = p_3 \tag{5}$$

Mixing Chamber (6)

In this section of the ejector, it is assumed that the primary and secondary flow will mix at a constant pressure equal to the pressure of the secondary flow at the suction line ($p_5 = p_6$). The properties in the mixing chamber can be calculated using the conservation of momentum and energy, as shown in Equation 6 and Equation 7, respectively.

$$v_6 = \frac{c_l(\dot{m}_1 v_3 + \dot{m}_4 v_5)}{\dot{m}_1 + \dot{m}_4} \tag{6}$$

[2] Ratio of the constant-area mixing section's throat to the primary nozzle's throat (Yan, Cai, & Li, 2012). In the case of the ejector at Theistareykir Geothermal Power plant, it had a converging nozzle and no constant area mixing section; therefore, the area ratio here is the ratio of the mixing chamber's throat (7) to the primary nozzle's exit (2).

$$h_6 = \frac{\dot{m}_1\left(h_3 + \frac{{v_3}^2}{2}\right) + \dot{m}_4\left(h_5 + \frac{{v_5}^2}{2}\right)}{\dot{m}_1 + \dot{m}_4} - \frac{{v_6}^2}{2} \tag{7}$$

Mixing chamber's throat (7)

As with the flow inside the primary nozzle, the flow in the mixing chamber is assumed to be isentropic. Thus Equations 8, 9, and 10 are used to calculate the fluid properties at the mixing chamber's throat.

$$\frac{A_7}{A_7^*} = \frac{1}{M_7}\left[\frac{1 + \frac{1}{2}(k-1){M_7}^2}{\frac{1}{2}(k+1)}\right]^{\frac{k+1}{2(k-1)}} \tag{8}$$

$$\frac{p_{7-0}}{p_7} = \left[1 + \frac{1}{2}(k-1){M_7}^2\right]^{\frac{k}{k-1}} \tag{9}$$

Given the isentropic efficiency η_n, and the isentropic enthalpy h_7^*, obtained from the calculated pressure and entropy, h_7 can be calculated as follows:

$$h_7 = h_6 - \eta_n(h_6 - h_7^*) \tag{10}$$

Diffuser (8)

The diffuser decelerates the fluid to recover the pressure. To calculate the properties at the diffuser's outlet, the steady one-dimensional incompressible continuity equation is used:

$$v_8 = v_7\left(\frac{A_7}{A_8}\right) \tag{11}$$

The enthalpy at the diffuser's outlet (h_8) can be obtained through energy balance, as shown in Equation 12, while the rest of the properties at the diffuser outlet are obtained by assuming that the entropy at the mixing chamber's throat is equal to the entropy at the diffuser outlet.

$$h_8 = h_7 + \frac{{v_7}^2}{2} - \frac{{v_8}^2}{2} \tag{12}$$

Figure 3 shows the flowchart of the analytical model of the ejector.

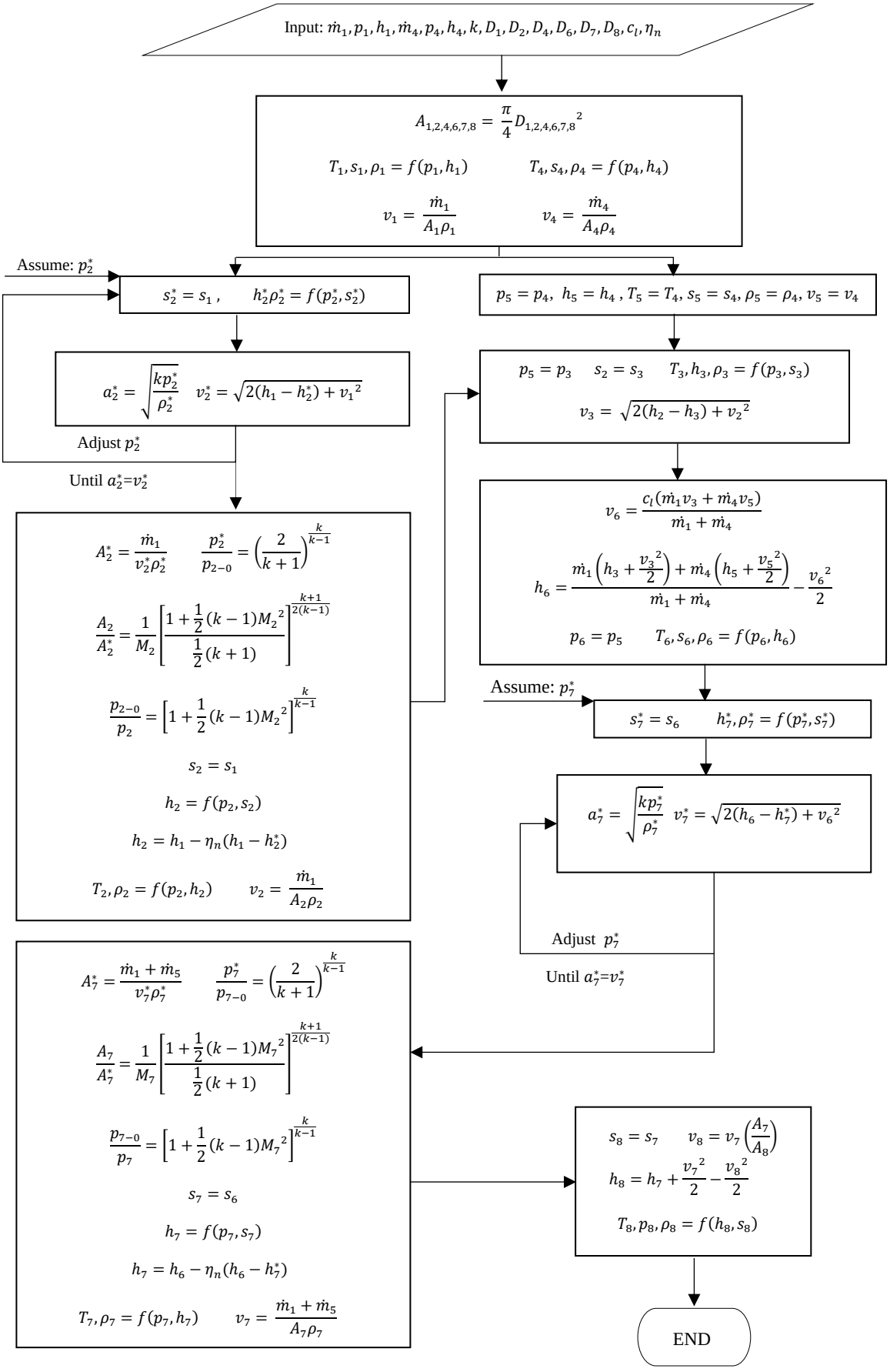

Figure 3. Flowchart of the analytical model of the ejector

4. EXERGY ANALYSIS

Exergy refers to the maximum useful work that can be produced from a specific heat source in a system at a given state in a specified environment (Valdimarsson, 2014). The total exergy of a flow (E_i) can be expressed in terms of the Kinetic exergy (E_{KE}), Potential exergy (E_{PE}), Physical exergy (E_{PH}), and Chemical exergy (E_O) as follows (Çengel, Boles, & Kanoğlu, 2019):

$$E_i = E_{KE} + E_{PE} + E_{PH} + E_O$$

Neglecting the potential and chemical exergies, the exergy can be expressed as (Çengel, Boles, & Kanoğlu, 2019):

$$E_i = (h_i - h_0) - T_0(s_i - s_0) + \frac{{v_i}^2}{2} \tag{14}$$

The subscript i denotes the evaluation point of the ejector, and the subscript 0 denotes the environmental state or the dead state, i.e., when the system is in thermodynamic equilibrium with the environment. For this analysis, the environmental state was assumed to be at an average pressure of 1 bar-a and 2.6°C, based on the location of the Theistareykir Geothermal Power Plant.

The exergy transfer or exergy rate by mass can be expressed as (Çengel, Boles, & Kanoğlu, 2019):

$$\dot{E}_i = \dot{m}_\iota \, E_i \tag{15}$$

Finally, the exergetic efficiency (ϵ_k) is the ratio of the desired exergy output of the ejector ($E_{P,K}$) to the exergy input of primary and secondary flows ($E_{F,K}$):

$$\epsilon_k = \frac{E_{P,K}}{E_{F,K}} \tag{16}$$

5. ANALYSIS OF MEASUREMENT DATA

The flow from well ThG-11 had an average enthalpy (h_1) of 2787 kJ/kg, and the pressure at the ejector inlet (p_1) ranged from 12.6 to 15.4 bar-g. Well ThG-15 had an average enthalpy (h_4) of 950 kJ/kg, and its ejector inlet pressure (p_4) ranged from 9.4 to 11.2 bar-g. The output of the ejector showed a variation in enthalpy (h_8) from 1637 to 2361 kJ/kg and pressure (p_8) from 9.9 to 11.5 bar-g, as shown in Figure 4.

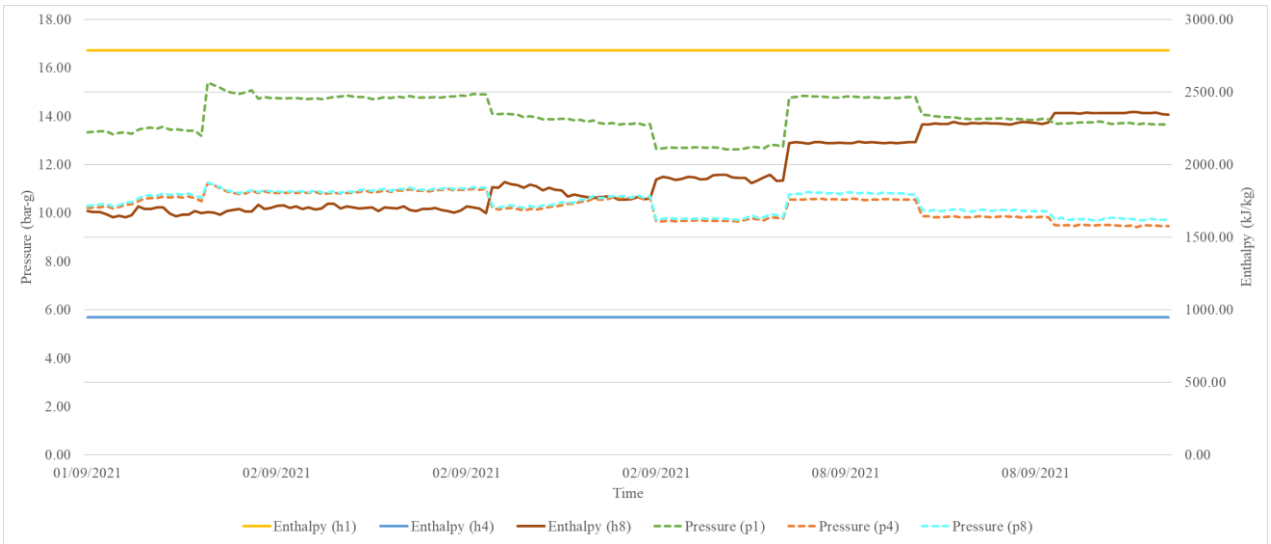

Figure 4. Enthalpy and pressure values of tested data

Figure 5 shows the correlation between the measurements of induced pressure from the secondary flow ($p_8 - p_4$) and the entrainment ratio (m_4/m_1). Test values with entrainment ratios higher than 0.8 had induced pressures less than 0.3 bar. On the other hand, entrainment ratios less than 0.5 were observed for induced pressures greater than 0.4 bar.

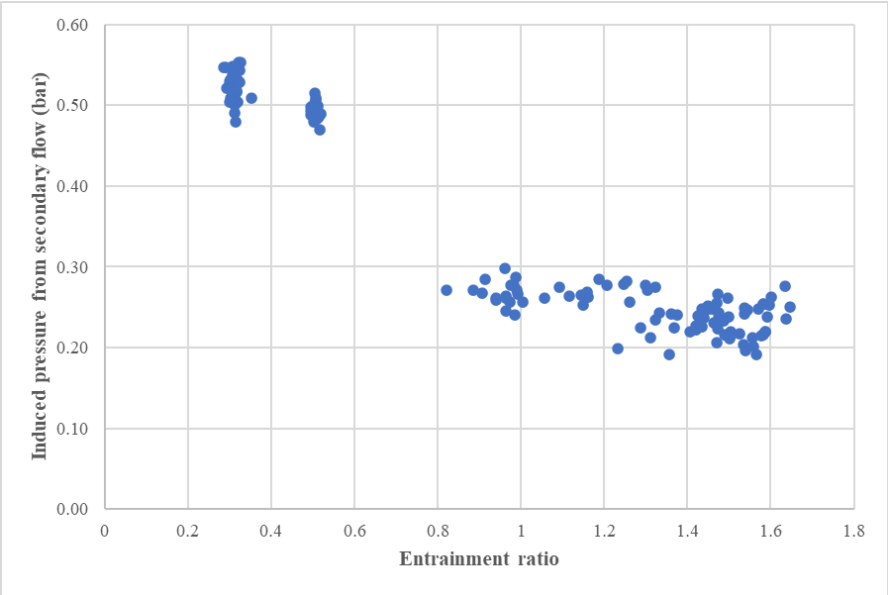

Figure 5. Relationship between induced pressure from the secondary flow and the entrainment ratio

Furthermore, the induced pressure varied depending on the difference between the primary and secondary flow's pressure ($p_1 - p_4$); as shown in Figure 6. More significant induced pressures (more than 0.4 bar) were obtained when the pressure difference between the primary and secondary flows was greater than 4.0 bar, except in the cases where the primary pressure was greater than 14.9 bar-g (values inside the red circle). This suggests that the tested ejector had a limit in the primary pressure inlet, which means that for greater pressures, like the ones achieved in real operation conditions of the power plant, a different design has to be made.

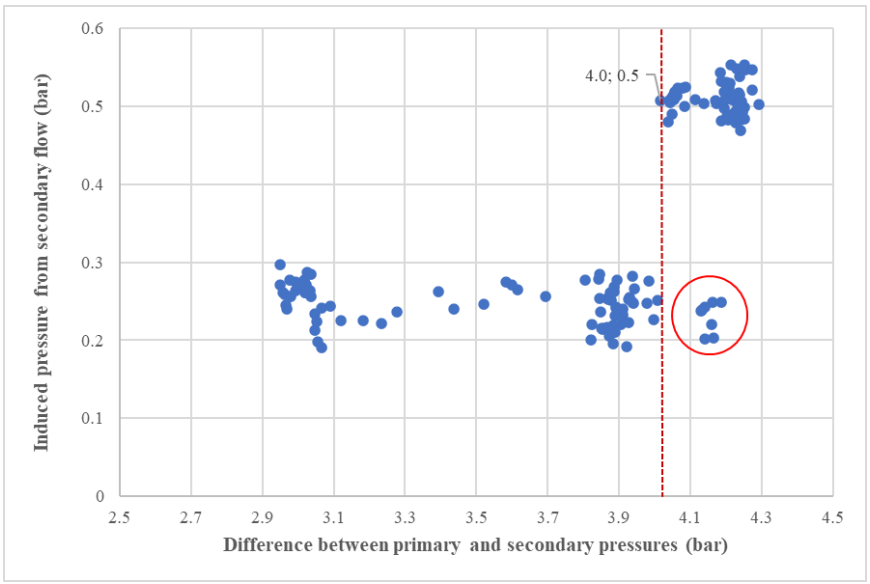

Figure 6. Relationship between induced pressure from the secondary flow and the difference between primary and secondary flow pressures.

Nevertheless, the added exergy to the system increased linearly with an increased entrainment ratio, see Figure 7. A good correlation coefficient (0.9) was observed. The highest exergy addition was found for an entrainment ratio of 1.6.

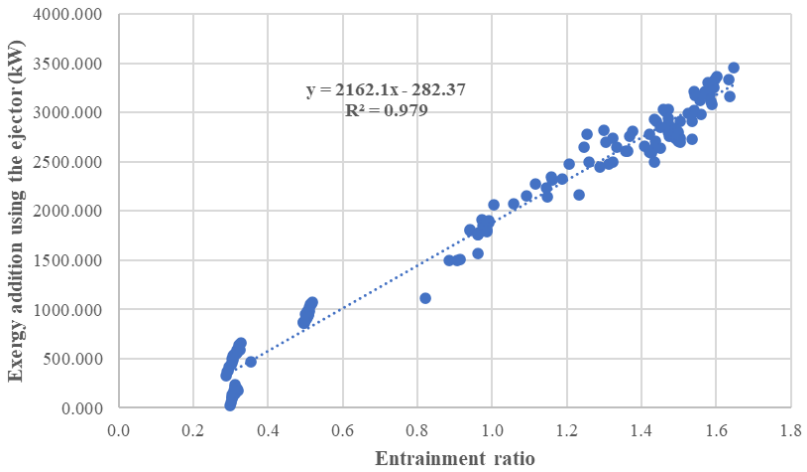

Figure 7. Relationship between entrainment ratio and exergy addition using the ejector

6. RESULTS

The ejector tested at Theistareykir Geothermal Power Plant had a subsonic behaviour, with a calculated Mach number of 0.2 at the outlet of the nozzle. The flow of steam in the converging nozzle accelerated with the subsonic value of M_2 as a function of the critical area ratio (A_2/A_2^*) (See Figure 3). Moreover, the pressure ratio (p_2/p_1) in that section was higher than the critical pressure ratio (0.5); therefore, the ejector failed to give the maximum primary flow discharge per unit area. For better understanding, a pressure-velocity profile was made, presenting the results of the analytical model as shown in Figure 8.

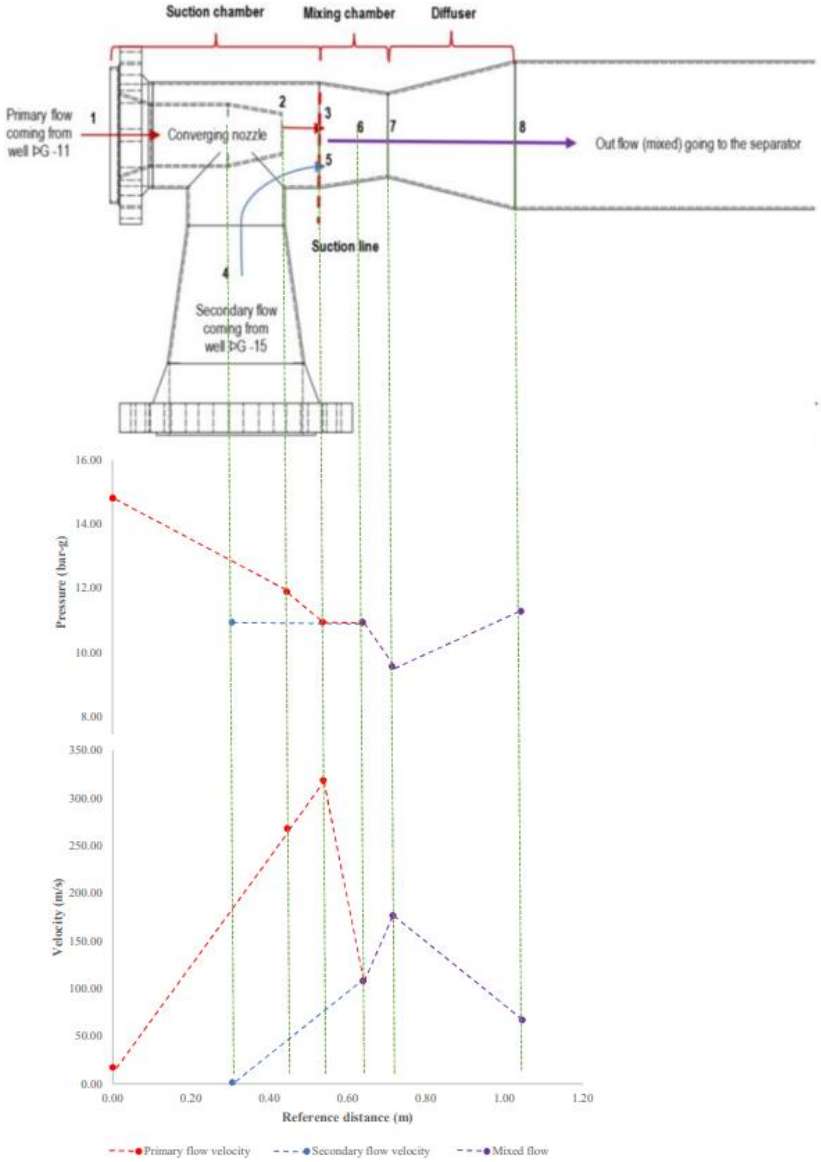

Figure 8. Pressure ad velocity profile of primary, secondary and mixed flows from the analytical model

The results from the analytical model show that the pressure at the primary nozzle exit (point 2) is higher than at the secondary inlet (point 4), i.e., the underpressure is not created there but must be created further downstream because, according to the test data, the ejector did entrain flow from the secondary inlet under these conditions. Preliminary CFD results indicate that the primary flow continues to expand downstream of the nozzle exit, with the pressure dropping below the secondary inlet pressure near the throat of the mixing chamber (point 7).

The mixed fluid accelerates as it passes through the mixing chamber's throat (from points 6 to 7), further decreasing the pressure. Finally, pressure is partially recovered as the fluid decelerates in the diffuser (points 7 to 8). The pressure and enthalpy at each step are illustrated on the P-h diagram in Figure 9.

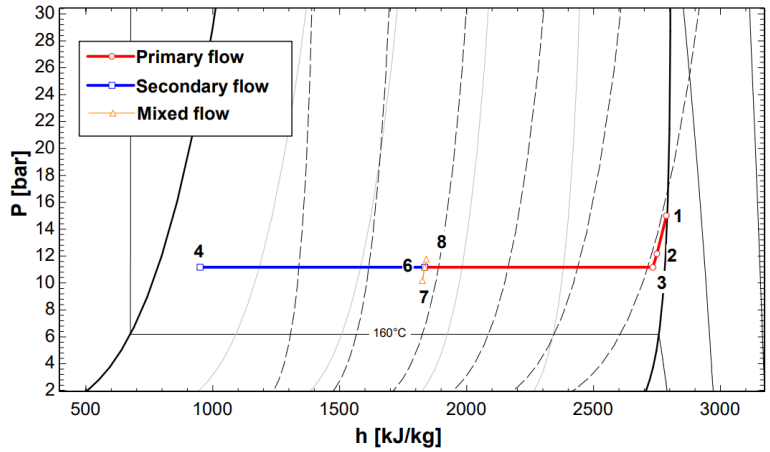

Figure 9. Pressure and enthalpy diagram of the ejector conditions tested at Theistareykir Geothermal Power Plant

Figure 10 illustrates the Grassmann diagram of the ejector, showing the exergy input and output, and exergy destruction according to the analytical model.

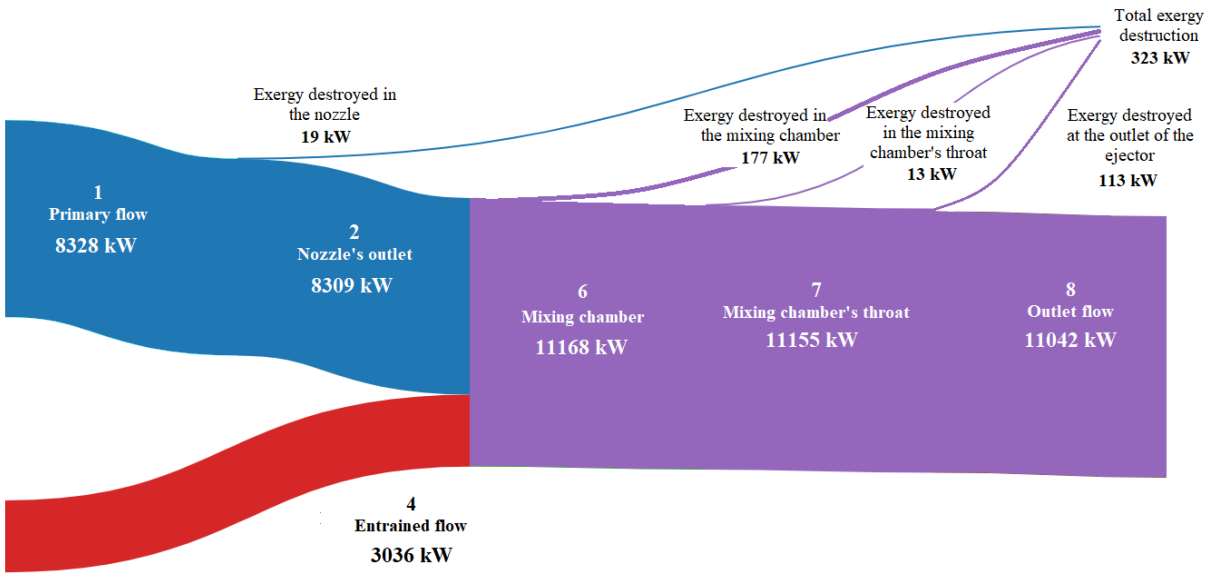

Figure 10. Grassmann diagram of the ejector tested at Theistareykir Geothermal Power Plant

There is minor exergy destruction in the nozzle's outlet due to the assumed isentropic efficiency ($\eta_n = 0.9$), which accounts for the internal friction between the steam and the nozzle. This friction is responsible for the enthalpy drop from the inlet to the outlet of the nozzle.

Moreover, there is greater exergy destruction in the mixing chamber, where the primary and secondary fluids mix with a reduction in enthalpy, entropy and velocity compared to the primary fluid at the outlet of the nozzle. Here, the coefficient for mixing and friction loss ($c_l = 84$) determines the deacceleration of the flow.

Finally, there is additional exergy destruction at the outlet of the ejector, as there is a slight increase in the enthalpy of the flow and a further reduction in velocity due to the increase in area at the diffuser section.

Despite the exergy destruction along the ejector, the maximum useful work that could be obtained from the system is still higher than the useful work obtained from the primary flow without using the ejector. An average of 1.69 MW and a maximum of 3.46 MW gained with the ejector were observed for the test conditions. Overall, the ejector's exergetic efficiency was 97%.

Figure 11 compares outlet pressure from test measurements and predicted values from the analytical model. The deviation of the model from the measured data ranges from -0.2% to +9.9%. The most significant error was found for those data series with less entrainment of the secondary fluid, which means less water coming in, so a smaller coefficient of friction loss than the one assumed in the model would be expected, and therefore, less outlet pressure. Further experimental tests and CFD simulations need to be executed to explain better the pressure behaviour under different conditions.

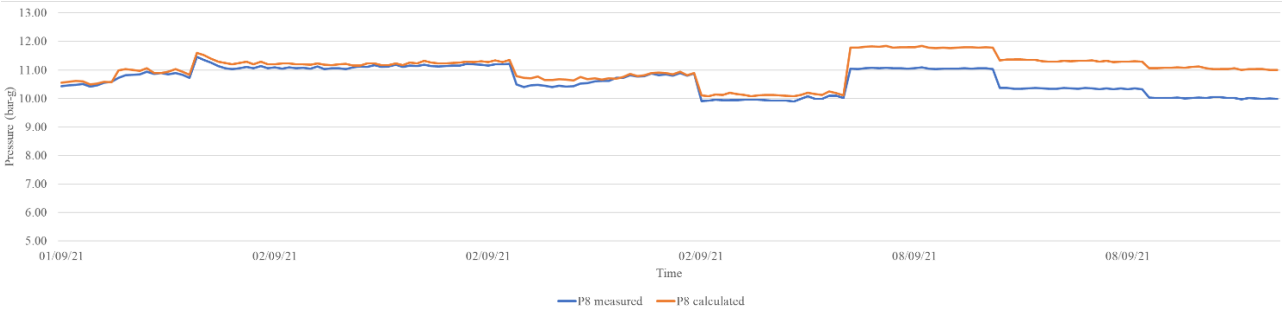

Figure 11. Comparison between measured and calculated outlet pressures

Figure 12 shows measured and calculated outlet enthalpy. The model shows a difference compared to the measured data ranging from -7.9% to +10.5%. The most significant discrepancies were noted when the entrainment ratio was greater than 1, which means that more mass flow from the secondary fluid was induced.

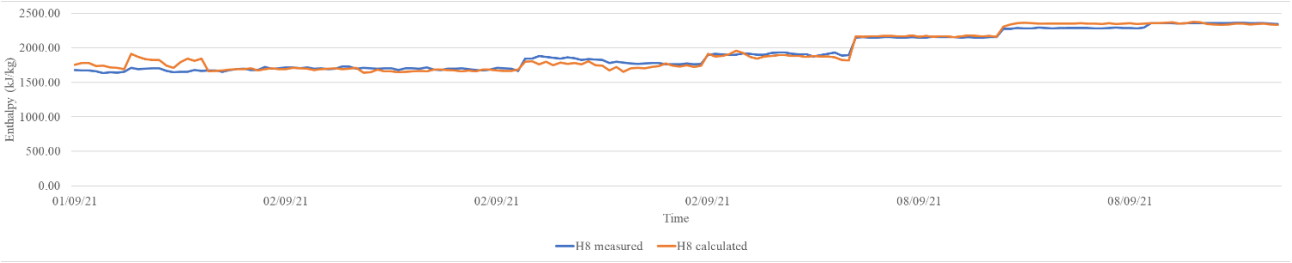

Figure 12. Comparison between tested and calculated outlet enthalpies

7. CONCLUSIONS AND RECOMMENDATIONS

- The ejector design tested at the Theistareykir Geothermal Power Plant in 2021 showed that an average of 1.69 MW and a maximum of 3.46 MW useful work could be obtained with the usage of the ejector under the test conditions.

- According to the model, the tested ejector had a convergent nozzle and operated under subsonic conditions. The average pressure reduction of the primary flow in the nozzle was 20.6%. This pressure reduction would be insufficient when the well ThG-11 operates under normal conditions, as the pressure difference between the nozzle outlet and entrained flow is expected to be more significant.

- The ejector used for the field test did not have a constant area mixing section that allows a proper mixing of the primary and secondary flows, with approximately uniform pressure. This setup is hard to predict using the analytical model resulting in higher pressure output difference in some cases.

- It is recommended that future field tests place more pressure gauges, mass flow meters and temperature sensors along the ejector to have more information about its behaviour. It is also desirable to have measurements for a sensitivity analysis under different pressure conditions.

- A good agreement between measured and calculated values was obtained with the analytical model, which predicts enthalpy better than pressure. Further experimental tests and CFD simulations must be executed to better explain the pressure behaviour under different conditions and analytical model scenarios.

- Generating underpressure from the primary flow to effectively entrain the secondary flow using the current setup is impossible in full-scale operation at the Theistareykir Geothermal Field. However, using a supersonic ejector with a converging-diverging nozzle could decrease enough the primary flow pressure at the outlet of the nozzle.

8. ACKNOWLEDGEMENTS

The authors would like to acknowledge Rannis Technology Development Fund, Project Number 2112948-0611.

9. NOMENCLATURE

A	Area (m^2)	E_O	Chemical exergy (kJ/kg or MJ/kg)
A^*	Critical area obtained when $M=1$ (m^2)	ρ	Density (kg/m^3)
a	Sonic velocity (m/s)	h	Enthalpy (kJ/kg)
c_l	Coefficient of friction loss	k	Constant specific heat ratio, 1.327
D_i	Diameter (cm)	$\dot{m}$	Mass flow (kg/s)
ϵ_k	Exergetic efficiency	Ma	Mach number

E_{KE}	Kinetic exergy	η_n	Isentropic efficiency of the compressible flow
E_i	Total exergy of a flow (kJ/kg or MJ/kg)	p	Pressure (bar-g)
$\dot{E}_i$	Exergy transfer or exergy rate by mass (kW or MW)	$p_{2,7-0}$	Stagnation pressure or the pressure at any point in the flow where the velocity is zero (bar-g)
$E_{F,K}$	Exergy input of primary and secondary flows (kJ/kg or MJ/kg)	s_i	Entropy (kJ/kg*K)
E_{PE}	Potential exergy (kJ/kg or MJ/kg)	T	Temperature (K)
E_{PH}	Physical exergy (kJ/kg or MJ/kg)	v_i	Velocity (m/s)
$E_{P,K}$	Desired exergy output of the ejector (kJ/kg or MJ/kg)		

9. SUBSCRIPTS

0 Environmental state or the dead state
1 Primary fluid at the entrance of the nozzle
2 Primary fluid at the nozzle's throat or nozzle's outlet (for a converging nozzle)
3 Primary fluid entering the mixing chamber (at the suction line)
4 Secondary fluid at the entrance of the ejector
5 Secondary fluid entering the mixing chamber (at the suction line)
6 Mixed fluid in the mixing chamber
7 Mixed fluid at the mixing chamber's throat
8 Mixed fluid at the ejector's outlet

10. REFERENCES

Anderson, J. Modern Compressible Flow with historical perspective, fourth edition. *McGraw-Hill Education*, New York, United States, (2021), 204–206.

Bell, I., Wronski, J., Quoilin, S., & Lemort, V. Pure and Pseudo-pure Fluid Thermophysical Property Evaluation and the Open-Source Thermophysical Property Library CoolProp. *Industrial & Engineering Chemistry Research*, (2014), 2498-2508.

Çengel, Y., Boles, M., & Kanoğlu, M. Thermodynamics: an engineering approach, ninth edition. *McGraw-Hill Education*, New York, United States, (2019), 438–484.

Ding, Z., Wang, L., Zhao, H., Zhang, H., & Wang, C. Numerical study and design of a two-stage ejector for subzero refrigeration. *Applied Thermal Engineering*, (2016), 436–448.

García del Valle, J., Sáiz Jabardo, J., Castro Ruiz, F., & San José Alonso, J. A one-dimensional model for the determination of an ejector entrainment ratio. *International journal of refrigeration*, (2012), 772-784.

Hardarson, F., Geirsson, S., Sveinsson, K., Einarsson, J., Sigurdsson, A., & Knutsson, V. Theistareykir Geothermal Power Plant, Description of the Steam Supply System: Design, Operation and Experience Gained. *Proceedings World Geothermal Congress 2020+1*. Reykjavik, Iceland (2021).

Huang, B., Chang, J., Wang, C., & Petrenko, V. A 1-D analysis of ejector performance, *International Journal of Refrigeration*, (1999), 354–364.

R. C., P., & Karamchandani, C. Elements of Heat Engines Volume II. *Acharya Publications*, Vadodara, India, (1994), 199–206.

Kumar Verma, S., Kumar, S., & Sachdeva, G. A review on exergy analysis of ejector refrigeration system. *Materials Science and Engineering*, (2021), 1–10.

Mkangala, A. Borehole Geology of Well ThG-15 at Theistareykir Geothermal Field, NE-Iceland. *Proceedings World Geothermal Congress 2020+1*. Reykjavik, Iceland, (2021).

Valdimarsson, P. Geothermal utilization – production of power. *Short Course VI on Utilization of Low- and Medium-Enthalpy Geothermal Resources and Financial Aspects of Utilization*. UNU-GTP and LaGeo. Santa Tecla, El Salvador. March 23-29, (2014).

IAPWS. *Revised Release on the IAPWS Formulation 1995 for the Thermodynamic Properties of Ordinary Water Substance for General and Scientific Use.* International Association for the Properties of Water and Steam, (2018).

White, F. Fluid mechanics, eighth edition. New York: *McGraw-Hill Education*, (2011).

Yan, J., Cai, W., & Li, Y. Geometry parameters effect for air-cooled ejector cooling systems with R134a refrigerant. *Renewable energy*, 155–163, (2012).